Coherent Structures in Transition of a Flat-Plate Boundary Layer at $Ma = 0.7$ *

ZHOU Ying(周莹)**, LI Xin-Liang(李新亮), FU De-Xun(傅德薰), MA Yan-Wen(马延文)

State Key Laboratory of Nonlinear Mechanics, Institute of Mechanics, Chinese Academy of Sciences, Beijing 10080

(Received 14 September 2006)

Direct numerical simulation (DNS) of a spatially evolving flat-plate boundary layer transition process at free stream Mach number 0.7 is performed. Tollmien–Schlichting (T-S) waves are added on the inlet boundary as the disturbances before transition. Typical coherent structures in the transition process are investigated based on the second invariant of velocity gradient tensor. The instantaneous shear stress and the mean velocity profile in the transition region are studied. In our view, the fact that the peak value of shear stress in the stress concentration area increases and exceeds a threshold value during the later stage of the transition process plays an important role in the laminar breakdown process.

PACS: 47. 27. Cn, 47. 27. De, 47. 27. nb

The study of the flat-plate boundary layer transition from laminar flow to turbulent flow is now one of the key problems in turbulence research. Physically understanding the mechanism in turbulence transition process is helpful to control the acoustic noise of aircraft and to reduce the friction coefficient over an aircraft's surface. Precisely predicting the starting point of turbulence transition has significant influence on the shape design and heat protecting arrangement of aircraft.

Throughout the transition process from laminar flow to turbulent flow, coherent vortex structures play very important roles. In recent years, there have been several investigations of the coherent vortex structures in transitional boundary layers. Ganapathisubramani *et al.*[1] performed particle image velocimetry (PIV) experiments and measured vortex packets in the logarithmic layer, finding that those vortex structures contribute a large part of Reynolds shear stress while occupying a rarely small area of the total. Zhou *et al.*[2] performed a direct numerical simulation (DNS) of the channel flow and investigated the generation mechanism of the coherent hairpin vortex packets, suggesting that an initial vortex exceeding a threshold strength can generate new hairpin vortices before and after the primary vortex and forms a coherent packet of hairpins which propagates downstream coherently. Suponitsky *et al.*[3] numerically studied the turbulent shear layers and their results have demonstrated that a small-amplitude initial disturbance evolves into a streaky structure, and a large-amplitude disturbance evolves into a hairpin vortex. Bake *et al.*[4] studied the mechanism of turbulence development in periodic Klebanoff transition by both experiments and DNS. They found that the interaction between vortical structures and high-shear layers can accelerate the transition to turbulence.

In this Letter, we perform the DNS of spatially evolving compressible flat-plate boundary layer transition process at free stream Mach number 0.7 by solving the compressible Navier–Stokes equations.[5] Typical coherent vortex structures in transition process are found in our results and the characteristics of those coherent vortex structures are discussed.

The inlet boundary condition can be written as

$$f(y,z) = \bar{f}(y) + \sum_{k=1}^{3} \varepsilon_k \hat{f}(y) e^{i(\beta_k z - \omega_k t)},$$

where f can be replaced by u, v, w, p, and T; $\bar{f}(y)$ is the steady flow profile obtained from two-dimensional laminar flat-plate boundary at $x = 30$ inch. The disturbances are a two-dimensional Tollmien–Schlichting (T-S) wave and a couple of conjugate three-dimensional T-S waves. The amplitudes ε_k, spanwise wave numbers β_k and frequencies ω_k are shown in Table 1; $\hat{f}_k(y)$ are corresponding eigen functions. The T-S wave parameters are obtained by using the code SAYR provided by Zhou Heng and Luo Jisheng at TianJin University.

Table 1. Disturbance parameters.

$\omega_1, \beta_1, \omega_1$	$\varepsilon_2, \beta_2, \omega_2$	$\varepsilon_3, \beta_3, \omega_3$
0.04, 0.00, 1.56	0.0005, 4.00, 1.56	0.0005, −4.00, 1.56

A non-slip isothermal boundary condition is used at the wall and non-reflecting boundary conditions are used at upper boundary and outflow boundary. The convection terms in compressible Navier–Stocks equations are approximated by a seventh-order accuracy upwind finite difference scheme, and the viscous terms are approximated by an eighth-order accuracy central finite difference scheme. The time evolution is carried out by the third-order TVD type Runge–Kutta method.[6]

The flow parameters and mesh parameters in the present computations are list in Table 2, where Ma_∞ is the free stream Mach number; Re_∞ is the free stream Reynolds number (using one inch as the length

* Supported by the National Natural Science Foundation of China under Grant Nos 90205025, 19872069, 170176033 and 10502052, and the Knowledge Innovation Project of Chinese Academy of Sciences under Grant No INF105-SCE.

** Email: gzhouying@gmail.com

unit); T_w is the temperature of the wall. The total number of computational mesh is $1000 \times 100 \times 320$. Fine mesh is adopted near the wall in the flat-plate normal direction. Uniform meshes are used in the streamwise and spanwise directions.

Table 2. Computational parameters.

Ma_∞	Re_∞	T_w
0.7	50000	1.098
$N_x \times N_y \times N_z$	$L_x \times L_y \times L_z$	$\Delta_x^+ \times \Delta y_w^+ \times \Delta z^+$
$1000 \times 100 \times 320$	$10.00 \times 0.65 \times 1.57$	$20.25 \times 1.013 \times 10.13$

Figure 1 shows the friction coefficient over the wall surface along the streamwise axis. The friction coefficient is defined as $C_f = \tau_w/(\rho\bar{u}^2/2)$, $\tau_w = \mu_w \partial\bar{u}/\partial y|_w$. The computational results are compared with the theoretical formula both at laminar section and at turbulent section in Fig. 1. Agreements between the computational and the theoretical results are good. The theoretical formula of friction coefficient for laminar flow is defined by Chen[7] as $C_{fL} = 0.6641/\sqrt{\mathrm{Re}_x}$, and the theoretical formula of friction coefficient for turbulent flow is defined by White *et al.*[8] as follows:

$$C_f = \frac{0.455}{S^2}\Big[\ln\Big(\frac{0.06}{S}\mathrm{Re}_x\frac{1}{\mu_w}\sqrt{\frac{1}{T_w}}\Big)\Big]^{-2},$$

$$S = \frac{1}{\sin^{-1}A}\sqrt{T_w - 1}, \quad A = \Big(r\frac{\gamma-1}{2}M_\infty^2\frac{1}{T_w}\Big)^{1/2}.$$

In the interval $x = 4.5$–8 between those two sections, there is a sudden increase of the friction coefficient from 0.0005 to 0.004. This is due to the appearance of three-dimensional vortex and the breakup of large-scale coherent structures in the transition process.

Figure 2 shows the normalized mean Van Direst velocity[8] profile at $x = 9.9$. The results show good agreements with both the wall law ($u^+ = y^+$) and the logarithm law ($u^+ = 25\log y^+ + 5.0$). Figure 3 shows the turbulent intensity profiles, which are normalized by the local mean streamwise velocity at $x = 9.9$, and the corresponding incompressible flow experiment data[9] are also plotted in Fig. 3. The DNS results are in good agreement with the experiment results. It is suggested that the compressibility effects are not so remarkable and Morkovin's hypothesis is tenable in our computation case.

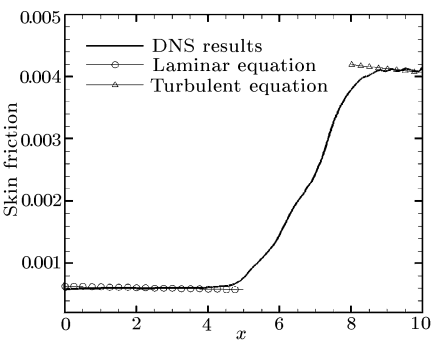

Fig. 1. Skin-friction coefficient along the flat-plate.

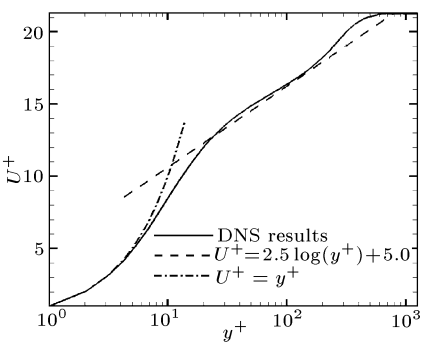

Fig. 2. Mean van Direst velocity profile normalized by wall shear velocity at $x = 9.9$ inch.

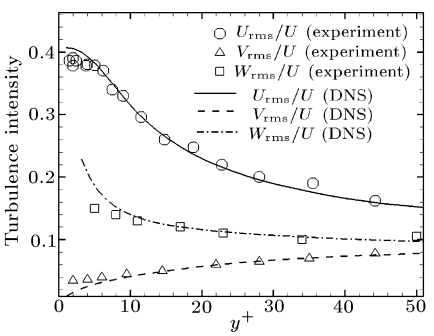

Fig. 3. Turbulence intensities normalized by local mean velocity at $x = 9.9$ inch.

Our attention focuses on the mechanism in the later stage of transition process and the evolvement of coherent structures in the laminar breakdown process. The DNS results show that when initial T-S waves propagate downstream with the mean flow, the secondary instability leads to the appearance of quasi-streamwise vortex (Λ vortex) and hairpin vortex.

Figure 4 shows the instantaneous isosurfaces of $Q = 10$ at different times. Here Q is the second invariant of the velocity gradient tensor, which is defined as follows:

$$Q = \Big(\frac{\partial u_1}{\partial x_1}\frac{\partial u_2}{\partial x_2} - \frac{\partial u_1}{\partial x_2}\frac{\partial u_2}{\partial x_1}\Big) + \Big(\frac{\partial u_1}{\partial x_1}\frac{\partial u_3}{\partial x_3} - \frac{\partial u_1}{\partial x_3}\frac{\partial u_3}{\partial x_1}\Big) + \Big(\frac{\partial u_2}{\partial x_2}\frac{\partial u_3}{\partial x_3} - \frac{\partial u_2}{\partial x_3}\frac{\partial u_3}{\partial x_2}\Big).$$

The Λ vortex is the precursor of hairpin vortex. The hairpin vortex first forms in near wall region and logarithm layer, then the head of hairpin vortex rises up and leaves the near wall region with the ejection of low-speed flow (Fig. 4(a)). The head keeps rising into a higher speed layer and is stretched and carried downstream by the shear stress of the mean flow. The vortex strength of the head becomes stronger because it obtains kinetic energy supply from the higher speed mean flow. Compared the pictures at different times in Fig. 4, it is found that the head of hairpin vortex moves faster than the hairpin vortex's leg in the streamwise direction. The head averaged convective velocity (in a time period) of the hairpin vortex head is 0.882, and the corresponding averaged convective velocity of the leg is 0.259. Because of the convective velocity difference between the head and the leg, the hairpin vortex continues becoming longer while it propagates downstream.

Based on our results and observation, the region where hairpin vortex located is closely related with high instantaneous Reynolds shear stress. This is con-

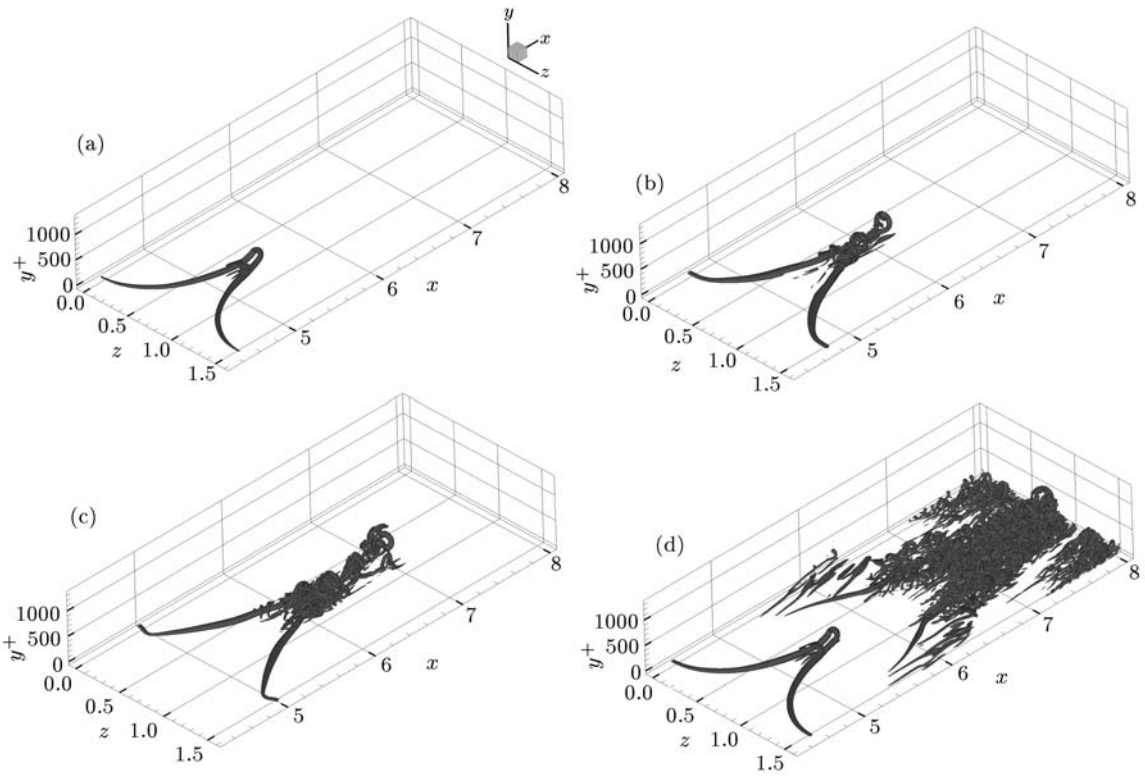

Fig. 4. Instantaneous isosurfaces of $Q = 10$ at different times: (a) $t = 15.61$, (b) $t = 16.62$, (c) $t = 17.63$, (d) $t = 27.69$.

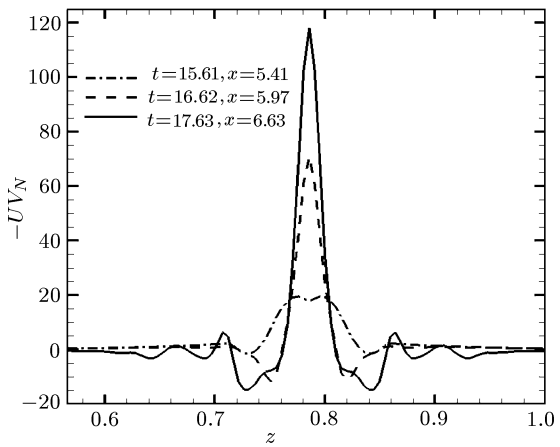

Fig. 5. Spanwise distribution of normalized shear stress $-UV_N$ at different times and at different locations.

sistent with the PIV experimental results of Ganapathisubramani *et al.*[1] Figure 5 shows the spanwise distribution of shear stress $-uv_N$ ($-uv_N = -uv/-\overline{uv}$) at the corresponding times of Figs. 4(a)–4(c) at the streamwise location of the hairpin vortex head, where $-uv$ is the instantaneous Reynolds stress and $-\overline{uv}$ is the Reynolds shear stress averaged on the $y - z$ plane at the same streamwise location. The hairpin vortex is stretched longer by the mean flow shear stress and its head rises higher away from the wall due to its own self-introduction during further development, and this in reverse leads to the shear stress around the head keeps increasing. After the shear stress exceeds a threshold value, the hairpin vortex breaks up at its neck area and forms a lot of new small-scale vortices around the breaking points (Fig. 4(b)). As it propagates downstream, the large-scale hairpin vortex becomes a packet of vortices (Fig. 4(c)). This whole vortex packet convects downstream integrally and is continually stretched by the mean stress. Then, all the large-scale structures break down into small-scale vortices, and form a turbulent spot. Finally, turbulent flow is formed after adjacent turbulent spots merge with each other (Fig. 4(d)).

Figure 6 shows the side views of Q isosurfaces. After the neck of hairpin vortex breaks up, the head sheds off from the hairpin vortex and forms an isolated and free vortex. The free vortex does not vanish quickly but propagates downstream along the outer layer of the turbulent boundary. Wang *et al.*[10] observed this process in their DNS of incompressible turbulent flow and it plays an important role in the energy transportation of boundary layer flow.

Figure 7 records the streamwise velocity oscillation at the point $x = 5.80$, $y^+ = 99.06$ (in the logarithm layer), $z = 0.79$ in a time period $t = 22.86$–26.86. During $t = 22.86$–24.40 the streamwise velocity curve is smooth, because the hairpin vortex has not passed this point yet. During $t = 24.40$–26.69 the curve oscillates heavily, this is because the hairpin vortex breaks up at its neck and breaks down into vortex packet during this period, then passes this point with the high frequency oscillation.

Figure 8 shows the velocity profiles along the streamwise axis in the interval $x = 4.5$–6.3, where the hairpin vortex locates at time $t = 24.18$ (Fig. 6(a)). In Fig. 8, the inflection points appear in the interval $x = 5.0$–6.0, and the deficit of velocity reaches the peak at $x = 5.8$, i.e. the location of hairpin vortex head (Fig. 6(a)). This is consistent with the suggestion of Huang *et al.*[11] Inflection points and the deficit of velocity disappear in the interval $x = 6.1$–6.3, because the flow is laminar in the area between the hairpin vortex and previous turbulent spot.

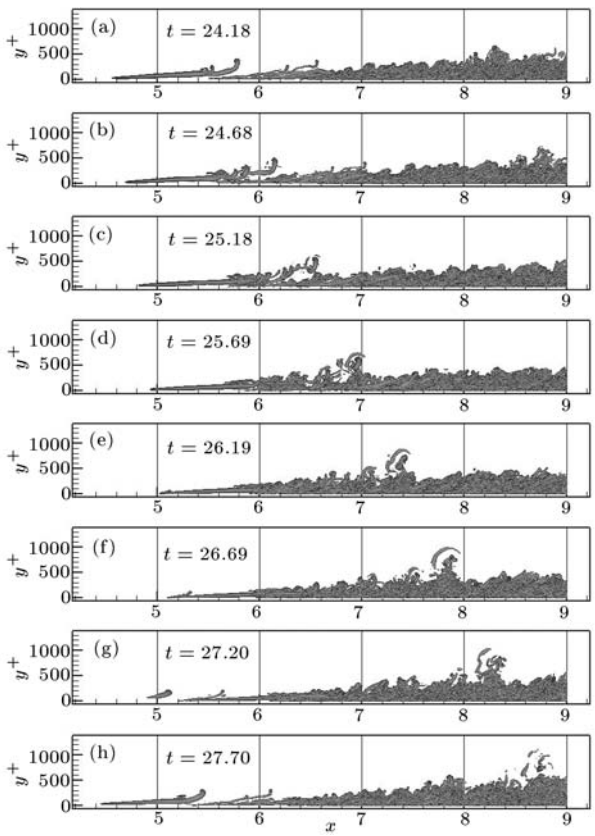

Fig. 6. Side views of instantaneous isosurfaces of $Q = 10$ at different instants in a time period.

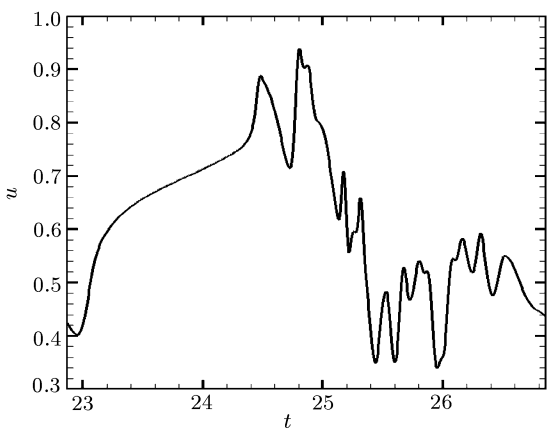

Fig. 7. Streamwise velocity along the time axis.

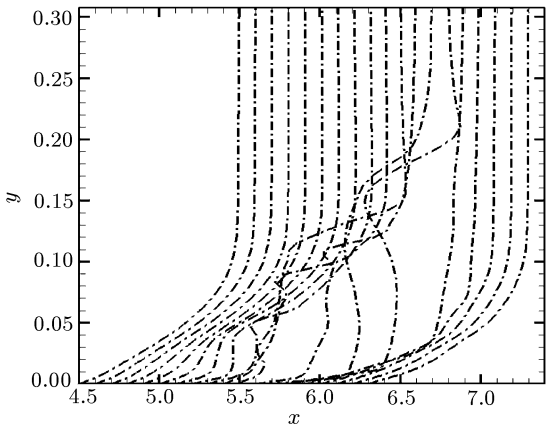

Fig. 8. Velocity profiles along the streamwise axis at $t = 24.18$.

In summary, we have carried out the DNS of a spatially evolving subsonic boundary layer transition from laminar flow to turbulence at $Ma = 0.7$. T-S waves are used as the inflow disturbances. Coherent vortex structures have been observed and discussed. It is found that breakup from large-scale structures to small-scale vortices is the beginning of the turbulent flow. Shear stress and velocity deficit are found to be concentrated both on the head and the breaking point of hairpin vortex. In our viewpoint, the fact that the peak value of shear stress in the stress concentration area increases and exceeds a threshold value during the later stage of the transition process plays an important role in the laminar breakdown process.

We thank Zhou Heng and Luo Jisheng at Tianjin University for providing the T-S wave code and helpful discussion on linear stability theory. We also thank the Supercomputing Centre of Chinese Academy of Sciences and the State Key Laboratory of Scientific and Engineering Computing for providing computation resources.

References

[1] Ganapathisubramani B, Longmire K and Marusic I J 2003 *Fluid Mech.* **478** 35
[2] Zhou J, Adrian R J, Balachandar S and Kendall T M 1999 *J. Fluid Mech.* **387** 353
[3] Suponitsky V, Cohen J and Bar-Yoseph P Z 2005 *J. Fluid Mech.* **535** 65
[4] Bake S, Meyer D G W and Rist U 2002 *J. Fluid Mech.* **459** 217
[5] Fu DX 2002 *Computational Fluid Dynamics* (Beijing: Higher Education Press) p 7
[6] Jiang G S and Shu C W 1996 *J. Comput. Phys.* **126** 202
[7] Chen M Z 2002 *Fundamentals of Viscous Fluid Dynamics* (Beijing: Higher Education Press) p 155
[8] White F M 1974 *Viscous Fluid Flow* (New York: McGrawHill)
[9] Fu S, Li Q B and Wang M H 2003 *Chin. Phys. Lett.* **20** 2193
[10] Wang M, Lele S K and Moin P 1996 *J. Fluid Mech.* **319** 197
[11] Huang Z F, Cao W and Zhou H 2005 *Sci. Chin.* G **48** 537